JGR Space Physics

RESEARCH ARTICLE
10.1029/2026JA035194

Temporal Variability of Saturn's H_2 Dayglow and Northern Aurora Observed by Hisaki and Cassini

L. S. Clare[1], S. V. Badman[1], T. Kimura[2], F. Tsuchiya[3], H. Tadokoro[4], C. Tao[5], Y. Kasaba[3], A. Bader[6], S. W. Farr[1], J. Kinrade[1], K. Yoshioka[7], A. Yamazaki[8], G. Murakami[8], I. Yoshikawa[9], and H. Kita[10]

[1]Department of Physics, Lancaster University, Lancaster, UK, [2]Department of Physics, Tokyo University of Science, Tokyo, Japan, [3]Planetary Plasma and Atmospheric Research Center, Graduate School of Science, Tohoku University, Sendai, Japan, [4]Department of Data Science, Tohoku Gakuin University, Sendai, Japan, [5]National Institute of Information and Communications Technology, Tokyo, Japan, [6]Gorillini NV, Antwerp, Belgium, [7]Department of Complexity Science and Engineering, Graduate School of Frontier Sciences, The University of Tokyo, Tokyo, Japan, [8]Institute of Space and Astronautical Science, Japan Aerospace Exploration Agency, Sagamihara, Japan, [9]Department of Earth and Planetary Physics, Graduate School of Frontier Science, The University of Tokyo, Tokyo, Japan, [10]Tohoku Institute of Technology, Sendai, Japan

Key Points:

- Significant temporal variability of Saturn's ultraviolet power over 3 weeks is detected by Hisaki and Cassini
- First analysis of the Hisaki observations of Saturn confirms that Hisaki is capable of detecting temporal behavior of the emission
- The emitted ultraviolet power is dominated by emission from the planetary dayglow which demonstrates strong correlation with solar activity

Correspondence to:
L. S. Clare,
l.clare@lancaster.ac.uk

Citation:
Clare, L. S., Badman, S. V., Kimura, T., Tsuchiya, F., Tadokoro, H., Tao, C., et al. (2026). Temporal variability of Saturn's H_2 dayglow and northern aurora observed by Hisaki and Cassini. *Journal of Geophysical Research: Space Physics*, *131*, e2026JA035194. https://doi.org/10.1029/2026JA035194

Received 5 FEB 2026
Accepted 22 MAY 2026

Abstract Ultraviolet (UV) emissions from molecular hydrogen in Saturn's atmosphere consist of bright auroral emission over the poles and disk-wide airglow. The dayside disk emits substantial intensities (dayglow) previously detected by various instruments. Exploration of dayside disk emissions provides insight into the interaction between the solar flux and planetary atmosphere. The respective contributions from the dayglow and the aurorae has not yet been evaluated, and the daily variability of the H_2 dayglow over timescales of weeks remains somewhat unexplored. For three weeks in 2014, the low-Earth orbiting telescope, Hisaki, monitored Saturn while Cassini concurrently observed Saturn's northern hemisphere from within the magnetosphere. The total emitted power varies by a factor of 2.26 over 23 days as observed by Hisaki, and 1.29 over 17 days by Cassini. Cassini data allow separation of the auroral power; the total power is dominated by that from the dayglow emission, with the northern aurora contributing ∼10%–26%. The disk-wide dayglow component displays strong correlation with solar activity, with Pearson correlation coefficients >0.8. The Cassini data further show that the global power at longer wavelengths (155–162 nm) depends more strongly on the solar spectrum than shorter wavelengths (70–148 nm). The auroral contribution to the total H_2 emission (70–170 nm) is ∼2%–14%. It is concluded that the total power is dominated by the dayglow from the disk, with solar photons controlling the H_2 dayglow emission.

Plain Language Summary Saturn's hydrogen atmosphere emits ultraviolet (UV) light from aurorae over the poles and dayglow from the dayside atmosphere. The dayglow is generated by the interaction of solar UV photons with the atmospheric hydrogen and is less explored than the aurorae at Saturn. Investigation of this emission will provide further understanding on the interaction between the activity from the Sun and the planet's atmosphere. Additionally, how the dayglow varies over time and how much the aurorae contribute to the overall emission is not well known. To address these questions, data from two missions, Cassini and Hisaki, are used to determine the total emitted power (both the dayglow and the northern aurora), and its variation over time. The total emitted power reveals significant variation over an approximately 3-week interval in 2014. The Cassini data allow the contribution from the northern aurora to be determined, which can be as much as 26%. Therefore, the total power is dominated by the dayglow contribution. Finally, the variation of the power is compared to the solar activity and it is concluded that the dayglow is controlled by this activity.

1. Introduction

Molecular hydrogen (H_2) ultraviolet (UV) emissions at Saturn have been detected from the atmosphere since the encounters by the Voyager probes in the 1980s, with the brightest intensities emitted from the aurorae. The auroral emission is generated by the acceleration of primarily magnetospheric electrons flowing along magnetic field lines, that then collide with atmospheric constituents (Lamy et al., 2013), demonstrating the interaction of the magnetosphere and the atmosphere. Outside of the auroral emission, the atmosphere emits airglow, with dayside intensities (often termed dayglow) observed to be higher than those on the nightside (Broadfoot et al., 1981). Exploration of the dayglow provides insight into the interaction between the solar extreme ultraviolet (EUV) flux

and the planetary atmosphere. Main UV emissions from the H-Lyman α line and the H_2 Lyman and Werner bands have been shown to correlate strongly with various indices for solar activity (Clarke et al., 1987; McGrath & Clarke, 1992).

Past studies aimed to identify the excitation mechanisms that generate such dayglow emissions. Broadfoot et al. (1981) demonstrated that the dayside disk UV emissions from Saturn were spectrally similar to those of Jupiter and that the integrated H_2 band intensity was a factor of 4 less than at Jupiter. This was quantitatively similar to the factor of 3.3 reduction of the solar flux from Jupiter to Saturn, demonstrating a solar control of the dayglow emission. Shemansky and Ajello (1983) investigated spectra of Saturn obtained by the Voyager 1 Ultraviolet Spectrometer (UVS), comparing H_2 bands observed on the dayside with electron excited H_2 synthetic spectra; electronic collisions were determined to contribute significantly to the intensities observed. Broadfoot et al. (1981) partially rejected the hypothesis that the observed H_2 emission was caused by photoelectrons, as this mechanism would require an unrealistically high conversion efficiency, with ∼65% of the solar photoelectron energy to be converted into the H_2 radiation alone. In order to explain this, Broadfoot et al. (1986) reasoned the need for an additional energy source and proposed electroglow, consisting of low energy charged particle excitation in the presence of sunlight that was entirely controlled by the solar flux (Yelle et al., 1987). Yelle et al. (1987) further suggested that electroglow was generated by solar fluorescence or the photolysis of H^- ions. Further exploration of two independent H_2 emission models by Yelle (1988), the first being excited by photoelectrons and the second by solar fluorescence, demonstrated that there were distinct differences between the spectral features of the emissions yielded. Using a combination of these two excitation mechanisms, Yelle (1988) obtained a good fit to Voyager UVS spectra of Jupiter, but with significant uncertainties due to poor spectral resolution. With improved spectral resolution in jovian spectra obtained with Hopkins Ultraviolet Telescope, Liu and Dalgarno (1996) concluded that the jovian H_2 dayglow emission could be entirely accounted for by a combination of solar fluorescence and photoelectron excitation.

In the case of Saturn, the study of the airglow using spectral data from the Cassini era is infrequently described compared to auroral studies. In the past, Voyager spectra have been analyzed to determine equatorial and central disk-average brightnesses (Broadfoot et al., 1981; Shemansky & Ajello, 1983; Yelle et al., 1986) as well as H_2 limb profiles (Yelle et al., 1986). More recently, Gustin et al. (2010) used limb-scan data from the Ultraviolet Imaging Spectrograph (UVIS) onboard Cassini and compared to a model of the H_2 airglow. They found that the electron impact process dominated the kronian airglow emission, with an average contribution of ∼68%, with the remaining approximately due to solar fluorescence. Despite this, they were unable to explicitly determine if solar fluorescence and photoelectron excitation are responsible for the airglow emission as for Jupiter, or if there is an additional energy source necessary. Although Broadfoot et al. (1981) initially partially rejected the photoelectron mechanism, Gustin et al. (2010) showed that a portion of the H_2 emission is generated by photoelectron impact excitation. Melin et al. (2009) explored the distribution of atomic hydrogen in the magnetosphere of Saturn, building mosaic intensity maps with Cassini UVIS spectral data. These mosaics reveal the partial dayside disk of the planet and a dependence of the H-Lyman α intensity on latitude and sub-solar latitude is suggested in their Figure 4. Stephenson et al. (2024) investigated the H-Lyman α airglow at Saturn using the extensive Cassini UVIS data set, determining that the emission from the disk is dependent on emission angle, incidence angle, latitude, and the solar flux at the top of the atmosphere; solar photons are therefore significant in the generation of the observed emission. They found that the observed H-Lyman α brightness exhibits a strong inverse dependence on the solar incidence angle, and comparison of temporal changes in the northern and southern hemispheres demonstrates a seasonal dependence. While this study analyses the H-Lyman α airglow, it demonstrates the need for further exploration to assess the response of the atmosphere to solar photons.

While previous studies provide insight into the mechanisms that generate this dayglow emission and the influence of the solar activity on atmospheric dynamics, no study has yet addressed the total power emitted from the dayside disk in the H_2 UV bands and the contribution of the aurora. The temporal variability of the dayglow also remains seldom explored, with previous studies investigating a small sample of spectra often focusing on spectral features. Numerous previous studies have established estimates for the emitted UV auroral powers (e.g., Bader, Badman, Cowley, et al., 2019; Clarke et al., 2005, 2009; Nichols et al., 2009), but there is a lack of global dayglow estimates. Quantification of the auroral contribution to the total power will aid in determining if the trends in total power are dominated by the dayglow or the auroral emission. The aurora is driven by particle precipitation and can significantly vary over short-timescales (∼hours). Separating the respective contributions will give insight

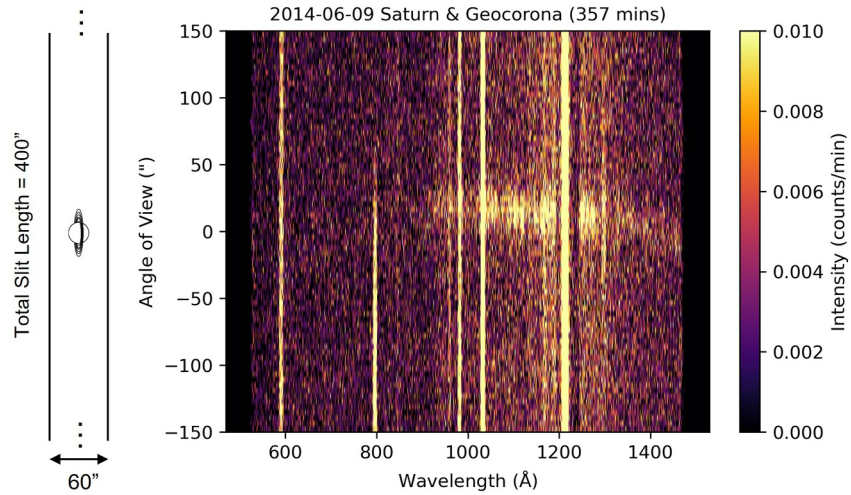

Figure 1. Two dimensional spectrum for the total (Saturn and geocorona) signal on 1 day of observation, totaling 357 min of integration time. The slit geometry is given to the left of the spectrum, with the approximate size of Saturn within the slit (not to scale).

into if the temporal trend is being driven by solar activity inducing an atmospheric response or enhanced particle precipitation over the auroral regions due to magnetospheric dynamics.

We set out to constrain the day-to-day variability over a period of 3 weeks, providing an opportunity to capture short-term trends and the atmospheric response to solar activity. We calculate the UV power emitted in the H_2 bands from the dayglow and north aurora at Saturn, comparing values from two coincident observation campaigns by Hisaki/EXCEED and Cassini UVIS in 2014. These will be compared to the solar activity to investigate the response of the atmosphere (Section 3). The contribution of the northern aurora is constrained. This study additionally presents a first analysis of the Saturn observing campaigns by Hisaki.

The long-term monitoring of the outer planets provides challenges such as increasing observer-target distances and observation period restrictions. Hisaki continuously observed Saturn and recorded spectral information at a high temporal resolution over a period of weeks. The campaign coincided with the Cassini mission, allowing a multi-mission comparison as is examined in this study. Using Hisaki observations is valuable in determining the robustness of such an instrument in monitoring Saturn, and will aid in the planning of Hisaki's potential successor, LAPYUTA (Tsuchiya et al., 2024). LAPYUTA is a candidate for JAXA's 6th M-class mission and one of the science objectives is solar system planetary atmospheres (Tsuchiya et al., 2026).

2. Observations and Analysis

This study compares findings from two different data sets taken by two different instruments, described respectively in Sections 2.1 and 2.2 below. Emitted UV powers are determined from Cassini UVIS observations and Hisaki/EXCEED observing campaigns. The total power is composed of the dayglow and auroral components; the dayglow component is referred to as the “disk” power in this study.

2.1. Hisaki/EXCEED Observations

We use observations of Saturn by the Hisaki satellite during two observing campaigns in 2014 DOY 143–167 and 2015 DOY 213–232; we focus on the 2014 campaign in this study. Hisaki was a JAXA spacecraft operating in low-Earth orbit, with a perigee of 950 km, an apogee of 1,150 km, and an orbital inclination of 31°. It was the first telescope to be completely dedicated to planetary science. The onboard payload was the EXCEED (EXtreme ultraviolet spectrosCope for ExosphEric Dynamics) spectroscope operating in the EUV wavelengths (Yoshioka et al., 2013; Yoshikawa et al., 2014), and a field-of-view guiding camera (Yamazaki et al., 2014). The spectroscope had three slit shapes and, during the observations of Saturn, the 60″ wide slit was selected. The data used in this study are Level-2 data products (Kimura et al., 2019), comprised of two dimensional spectra of 1,024 spatial pixels by 1,024 spectral pixels covering wavelengths of 52–148 nm (as seen in Figure 1). The spatial

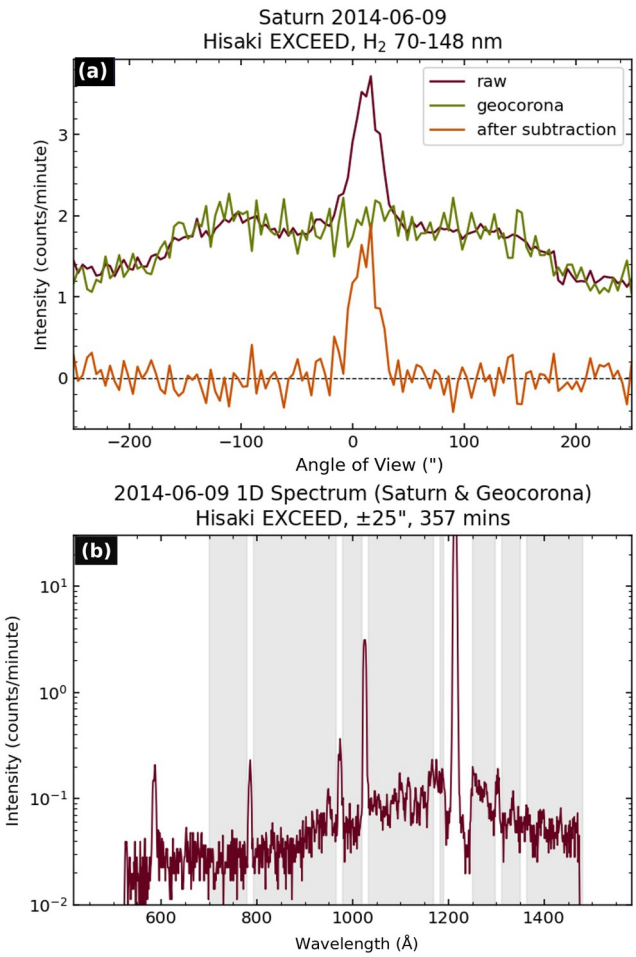

Figure 2. The geocoronal subtraction, and the selection of spatial and spectral regions. (a) Spatial-intensity profiles of the total signal (purple, "raw"), geocoronal signal (green, "geocorona"), and the resulting subtraction (orange) for 2014 DOY 160. The signals are integrated over the wavelengths of interest highlighted in the panel below. The signal from Saturn is visible as a peak near 0″. (b) One dimensional spectrum of the total signal for 2014 DOY 160; the counts are spatially integrated between ±25″. The H_2 Lyman and Werner bands are shown in the gray shaded regions; geocoronal atomic hydrogen, oxygen, and nitrogen lines, as well as the narcissistic ghost are excluded from the wavelength range of interest.

resolution of the instrument was 17″ with a spatial plate scale of 4.1″/pixel, and the slit's spectral resolution was 0.7–1 nm at Full Width at Half Maximum (FWHM) and one pixel along the wavelength axis was approximately 0.11 nm, high enough to separate planetary EUV emission lines (Kimura et al., 2019; Yoshioka et al., 2013).

The spatial region of interest to this study is ±25″ around the slit center, corresponding to the intensity feature visible in Figure 2a. In this case, 50″ is equivalent to ~5 R_S (R_s = Saturn radii). Due to the spatial resolution of the instrument being comparable to the diameter of Saturn, it is not possible to spatially isolate Saturn's auroral emission with Hisaki. The spectral region we focus on are the H_2 bands in the range 70–148 nm. Due to the nature of Hisaki's orbit, the data are subject to contamination from the geocorona which must be removed to determine the total emission power from Saturn. We remove geocoronal emission lines at 97.2 nm (H-Lyman γ), 102.6 nm (H-Lyman β), 117.5 nm (NI), 121.6 nm (H-Lyman α), 130.4 nm (OI), and 135.6 nm (OI). The narcissistic ghost at 78.6 nm is also ignored (Yoshikawa et al., 2014).

We determine the geocorona observations by selecting intervals where the local time (LT) of Hisaki was between 19 and 05 hr during a calibration event, when the spacecraft pointed several arcminutes off-target. The spectra corresponding to these times are summed and then divided by the geocorona integration time. Determination of Saturn observation times (with the geocorona contamination) is performed in a similar fashion, by selecting times when the spacecraft was outside of a calibration event but within the 19-05 LT range. In order to remove the geocoronal signal, we subtract from the total signal and obtain the Saturn-only signal, as demonstrated by Figure 2a. However, due to a wavelength-dependent instrumentation effect, the spectral features are off-axis (visible in Figure 1) and require calibration to align them with the slit center, and bring the H_2 emissions into the spatial region of interest. Slices at each spectral pixel are taken and a Gaussian is fitted to the intensity distribution. The data are then shifted toward the slit center using the offset of the Gaussian peak for each slice, aligning the emission features.

The total emission power per observation day is derived according to Kimura et al. (2019), given in Equation 1, where P is the emitted power in Watts, R is the observer-target distance at the observation time in meters, E_i is the photon energy at the i^{th} wavelength pixel in Joules, A_i is the effective area of the detector at the i^{th} wavelength pixel in square meters, Δt is the temporal resolution in seconds, and C_i and G_i are the spatially integrated source and background counts at the i^{th} wavelength pixel. We assume an isotropic emission source over 4π steradian. Days with <100 min of integration time and/or negative powers are removed from the analysis.

$$P_{\text{Hisaki}} = \sum_i \frac{4\pi R^2 E_i}{A_i \Delta t}(C_i - G_i) \quad (1)$$

2.2. Cassini UVIS Imagery

This study uses a sequence of complementary auroral imagery from the Cassini Ultraviolet Imaging Spectrograph (UVIS) (Esposito et al., 2004); Cassini made multiple observations of Saturn's aurorae during its 13 years in orbit, but we utilize 896 auroral images from the northern hemisphere in the interval 2014 DOY 145–162. Pseudoimages were obtained with the FUV and EUV spectrographs by scanning the 1.5 × 64 mrad FUV slit and the 2 × 64 mrad EUV slit simultaneously across the region, with multiple scans often necessary to cover the region of interest. The median exposure time of each pseudoimage employed here ranges from 9.2 to 11.9 min. The

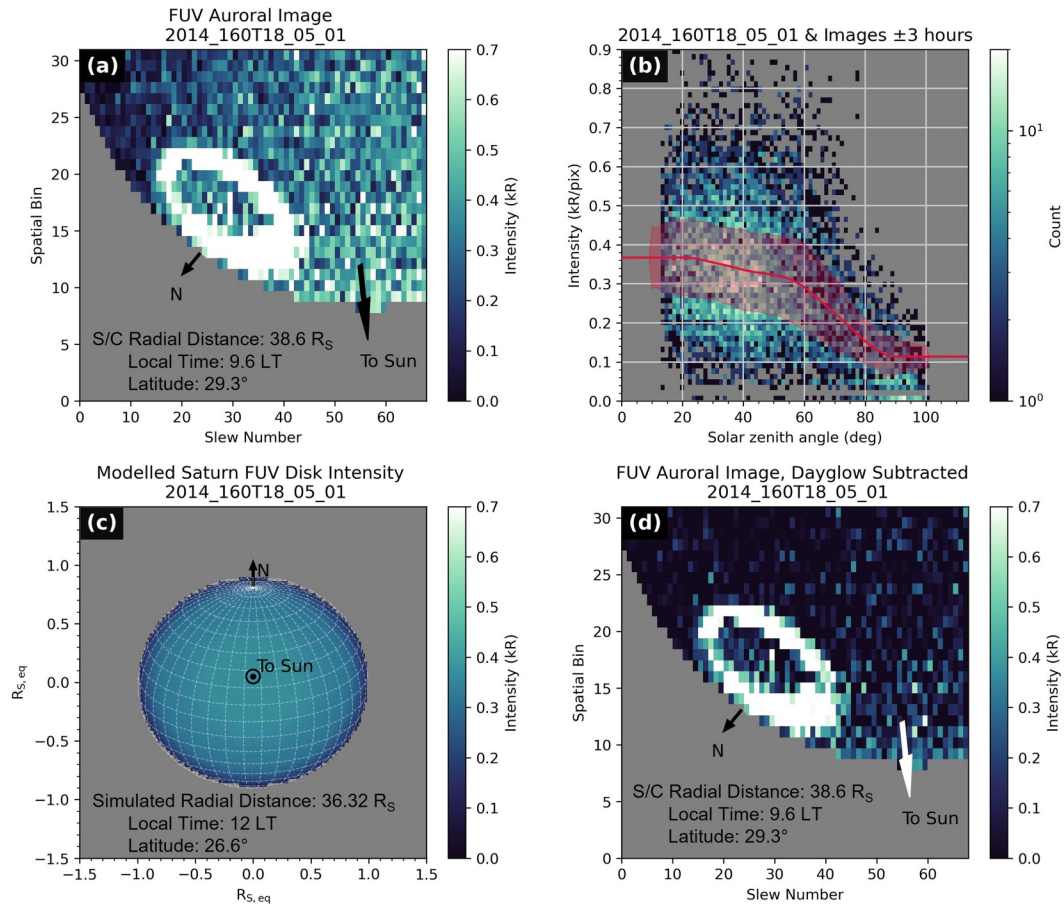

Figure 3. Estimation of the dayglow intensity in Cassini UVIS observations. (a) A calibrated and spectrally integrated FUV UVIS auroral image; the orientation of the north pole, the direction toward the Sun, and the spacecraft's position are indicated. The FUV range of the H_2 intensity is given by the color bar to the right. (b) SZA-brightness histogram of the FUV dayglow emission of images that are within ±3 hr of the selected image; the median filtered data are shown in red and the associated median absolute deviation is shown by the shaded red region. (c) FUV dayglow brightness map estimation and interpolation. The view is modeled as from the Sun-Saturn line at the sub-solar latitude with the north pole of Saturn at the top. The simulated position of the spacecraft is given. (d) The dayglow-removed auroral image. FUV, Far Ultraviolet; UVIS, Ultraviolet Imaging Spectrograph; SZA, Solar Zenith Angle.

detected intensities in the EUV and FUV channels are separately calibrated. We spectrally integrate the EUV data from 70 to 118 nm and the FUV data from 118 to 148 nm, avoiding the same atomic lines as those in the Hisaki analysis. This choice will allow a direct comparison of the resulting emitted powers between Hisaki and Cassini data.

The northern auroral images include dayglow emissions, as Saturn was in northern summer during the interval studied here. The sub-solar latitude was 26.6°. The auroral images do not cover the entire dayside disk visible from Earth orbit during this time, requiring an estimation of the H_2 dayglow brightness on the planetary disk in order to determine the total emitted H_2 UV power. The method of estimating the dayglow brightness from the UVIS imagery employed in this study is similar to that of Bader, Badman, Yao, et al. (2019); Bader, Badman, Cowley, et al. (2019). Images that are within ±3 hr of the selected image (Figure 3a) together with the solar zenith angle of each image pixel (SZA; determined using SPICE) are used to determine a brightness dependence on SZA (Figure 3b). An SZA-brightness histogram is constructed, not including the auroral pixels (colatitudes of <25°) or pixels on the limb. The data are then median filtered with a box 10° wide in SZA, and a brightness dependence is determined. In order to determine the brightness profile of the disk as it would be seen along the Sun-Saturn line at a fixed radial distance, the solar zenith angle is determined at each synthetic grid pixel on an oblate spheroid disk.

Using the constructed solar zenith angle map, the planetary disk brightness map is modeled (Figure 3c). This procedure is repeated separately for the FUV and EUV integrated intensities.

The auroral images and the modeled disk brightnesses are treated separately when calculating the emitted powers. The emitted power is determined by Equation 2 (Groulard et al., 2024; Gustin et al., 2012), where P is the emitted power in Watts, I_j is the intensity in kR per j^{th} image pixel and multiplying by 10^9 gives photons cm^{-2} s^{-1}. The term $\delta\theta$ is the angular change of the boresight per slew in mrad, and the size of a spatial pixel in mrad is l_{spat}. The observer-target distance at the observation time in km is R, E_{photon} is the mean photon energy in the wavelength range in Joules, and the factor 10^{10} allows conversion from km^2 to cm^2. An isotropic emission source over 4π steradian is assumed. In this interval, both the FUV and EUV imagery were rebinned onboard Cassini from 64 to 32 spatial bins, and from 1,024 to 64 spectral bins for 2014 DOY 145–160 and to 32 spectral bins for 2014 DOY 161 and 162.

$$P_{\mathrm{UVIS}} = \sum_j I_j E_{\mathrm{photon}} l_{\mathrm{spat}} \delta\theta R^2 \left(\times 10^9 \times 10^{10}\right) \quad (2)$$

For the modeled disk images, the observer-target distance is fixed and pixels at SZA < 90° are selected. The FUV disk power and EUV disk power is calculated according to Equation 2. In the case of the auroral images, the brightness dependence is used to subtract the dayglow (Figure 3d), to avoid double counting the pixels outside the aurora. The observer-target distance is the radial distance of Cassini at the observation time (determined using SPICE); only auroral pixels covering 8–22° colatitude and on the dayside are selected and input into Equation 2 to obtain FUV and EUV auroral powers. To determine the total power over the selected H_2 wavelengths, the FUV and EUV powers are summed.

Additionally, the analysis is performed for the total H_2 intensity (70–170 nm), by integrating the emission intensity in the wavelength range 155–162 nm (FUV channel only) and multiplying by an empirical factor of 8.1 (Bader, Badman, Cowley, et al., 2019; Gustin et al., 2016, 2017). This empirical factor is based on a H_2 spectrum generated by keV primary electron impact (Gustin et al., 2004) which is more appropriate to the auroral regions than the disk dayglow. However, many studies investigating H_2 emission at Saturn often refer to a total H_2 emission intensity in this wavelength range; performing this procedure for this wavelength range allows comparison to previous studies. We will refer to 70–148 nm as the "short band" and 70–170 nm as the "extended band."

3. Results and Discussion

This section presents the first quantitative analysis of Saturn's H_2 ultraviolet emission observed by Hisaki/EXCEED, and compares these results with coincident, archival measurements from Cassini UVIS. Emitted UV powers in the H_2 bands have been determined from Hisaki for the wavelength range 70–148 nm (excluding atomic hydrogen, nitrogen, and oxygen), and from Cassini for the same selected H_2 bands as Hisaki (short band) and for the total H_2 wavelength range 70–170 nm (extended band). The Hisaki mean UV power over the interval is 53.5 ± 9.5 GW, compared to 93.4 ± 6.6 GW from Cassini which is a factor of 1.7 larger. The use of Cassini imagery allows the auroral component to be separated and an estimation of its contribution to the total power.

3.1. Total Emitted UV Power Derived From Hisaki/EXCEED

The total emitted power determined from the Hisaki/EXCEED observations is presented in Figure 4a; the errors are estimated using Poisson statistics. A general increase in the power is observable from 41.1 ± 2.3 GW on 2014 DOY 144 to 69.6 ± 3.8 GW on 2014 DOY 162. A decrease in the emitted power then follows to the end of the interval on 2014 DOY 167. Overall, the power varies by a factor of ∼2.26 during this interval. These emitted powers are representative of the dayglow from the disk, northern aurora, and reflection of sunlight from the rings; it is not possible to separate the contributions due to the limited spatial resolution of EXCEED. Hisaki further observed Saturn in August 2015 but no coincident Cassini data are available for this interval. However, the same analysis for these data are performed and the results are reported in Appendix A.

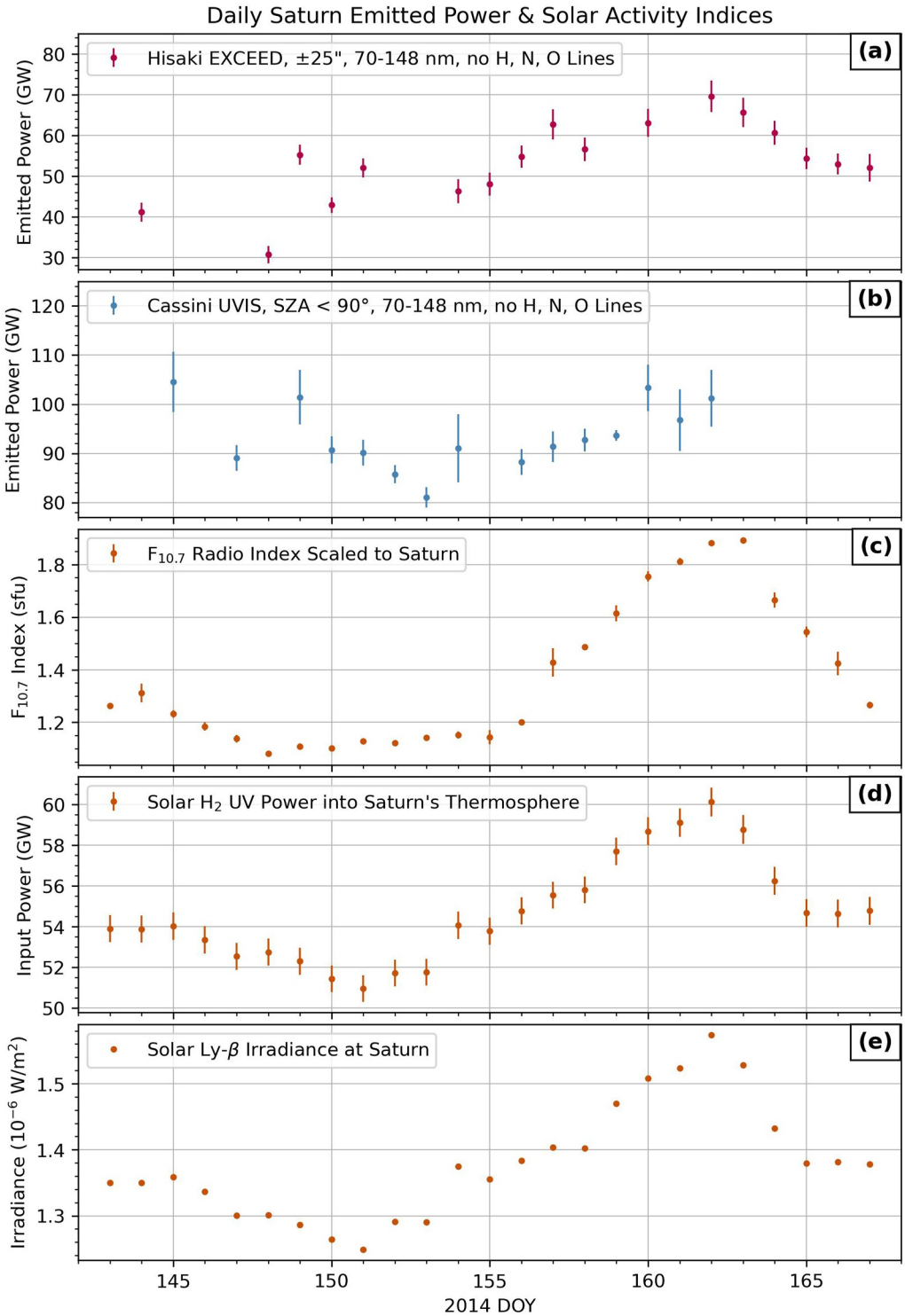

Figure 4. A summary of the total emitted power and solar indices for the 2014 interval. (a) The total emitted UV power obtained from Hisaki/EXCEED. The points are daily average H_2 powers from 70 to 148 nm. (b) The total emitted UV power determined with Cassini UVIS; each point is the daily average H_2 power for the wavelength range 70–148 nm. (c) The daily average solar $F_{10.7}$ radio index, which acts as a proxy for EUV radiation, scaled to Saturn. Data from Space Weather Canada. (d) The solar EUV power into Saturn's thermosphere. Solar spectral irradiance data are obtained from LISIRD, which uses the Flare Solar Irradiance Model (Chamberlin et al., 2008) and Earth irradiance measurements. The calculation is from Gershman and DiBraccio (2024). (e) The solar H-Lyman β irradiance at Saturn; data are obtained from LISIRD, which uses the Flare Solar Irradiance Model (Chamberlin et al., 2008) and Earth irradiance measurements. The uncertainty on the solar H-Lyman β irradiance ranges from 22.9% to 26.2% over the interval.

3.2. Comparison With Cassini UVIS Measurements

Total emitted powers from the dayside disk and northern aurora are derived from Cassini UVIS data in the same wavelength ranges used in the Hisaki analysis, in order to allow a direct comparison between the instruments and assess the robustness of Hisaki for observations of the outer planets. The powers determined are daily average values, to compare to the daily Hisaki power, and are presented in Figure 4b; the errors are the standard deviation, which gives an indication of variability within 1 day. Previously, Bader, Badman, Yao et al. (2019) estimated that the uncertainty in their UV auroral power per pseudoimage, using the FUV UVIS channel data and the method from which this study derives, was likely only a few GW. Additionally, the calibration procedure for the FUV spectrograph is known to be within an uncertainty of 15% (Gustin et al., 2017).

While the Cassini powers are often the same order of magnitude as those of Hisaki, they are consistently larger. Over the 2014 interval, the Cassini total power generally trends downwards until 2014 DOY 148 before following a similar increase in power as observed with Hisaki. The total emitted power peaks on 2014 DOY 145 at 104.6 ± 6.1 GW, before decreasing to a lower power on DOY 147 and rising again on DOY 149. There are no suitable data from Hisaki on DOY 145 or 147 but a similar trend is observed, with a lower power on DOY 148 rapidly increasing on DOY 149. It can also be seen that, while the emitted power derived from Cassini data does not peak on DOY 162, the powers on DOY 145, 149, and 162 are within one standard deviation of each other. The Cassini power varies by a factor of ∼1.29. The coverage of Cassini data does not extend beyond DOY 162.

A difference of ∼1.7 between the Cassini UVIS power and Hisaki/EXCEED power can be attributed to several factors: the spectral resolution of Cassini UVIS is 0.48 nm (Esposito et al., 2004) without spectral binning, higher than that of Hisaki; the geocoronal signal subtraction step in the Hisaki processing resulted in some pixels possessing a negative intensity value and these pixels were not rejected in the determination of power, leading to a potential general underestimation; there are different calibration procedures applied and cross-calibration between UV instruments is difficult (e.g., Koskinen et al., 2020). The difference between the two instruments is not unexpected; Kita et al. (2019) found a factor of ∼8 difference between Jupiter's auroral power determined by Hisaki and Juno, with the Juno auroral powers consistently around an order of magnitude larger, reasoning differing wavelength ranges and a longitudinal modulation correction. Additionally, Kimura et al. (2015) found that jovian auroral power determined by Hisaki and HST differed by a factor of ∼3, also due to differing wavelength ranges. Although these studies focused on Jupiter, this factor of ∼1.7 difference that we see in this study appears to be reasonable. Furthermore, this study assumes a uniform, linear profile of the modeled dayside disk brightness, whereas the actual dayside disk appears banded in HST UV imagery (see Figure 1 in Gérard et al. (2004), e.g.). This may contribute to the differences in values and trend observed in the Hisaki and Cassini powers. While the Cassini powers are limited to the planetary disk and northern aurora, they do not take the rings or the ring shadow into account. The ring shadow was not visible from Earth during the interval, due to the season at Saturn, and the total power should be a reasonable approximation. In the case of the Hisaki observations, reflection of sunlight from the rings themselves is detected, whilst the ring contribution is not included in the Cassini values. Therefore, a portion of the power calculated from Hisaki observations will be likely be from sunlight reflected from the rings.

Additionally, the same process described in Section 2.2 is repeated for the extended band. Figure 5a presents the total emitted power from the disk-wide dayglow and northern aurora for these wavelengths. The values are an order of magnitude greater than Hisaki/EXCEED. The total power increases steadily from 591 ± 25 GW on DOY 145 and peaks on DOY 162 at 897 ± 32 GW.

3.3. Solar Activity Dependence

Three proxies for the solar activity are selected for comparison to UV emitted power. The $F_{10.7}$ radio index serves as a proxy for solar EUV radiation (Tobiska et al., 2008). The solar EUV power at Saturn is determined using solar spectral irradiances from the Flare Solar Irradiance Model via LISIRD (Chamberlin et al., 2008), which are input into the calculation for solar EUV power from Gershman and DiBraccio (2024), in the same wavelengths selected in the Hisaki analysis. Finally, the solar H-Lyman β irradiance at Saturn over the interval is determined using the same Flare Solar Irradiance Model via LISIRD. Their temporal variabilities in the same interval are presented in Figures 4c–4e. The solar activity indicators demonstrate an increase over time, peaking on DOY 162 (DOY 163

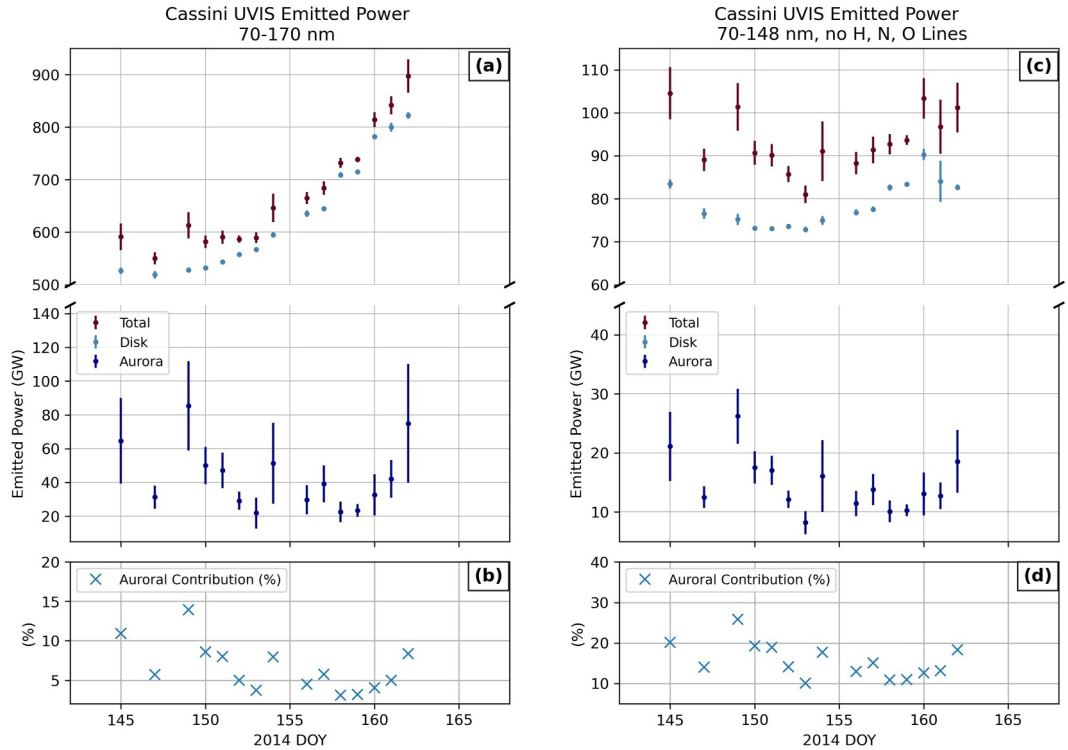

Figure 5. The variation of the Cassini UVIS disk and auroral powers over the interval. (a) The total emitted power from the disk and northern aurora, the disk only, and the northern aurora (between 8° and 22° colatitude, dayglow subtracted) for the extended band. (b) The percentage contribution of the northern auroral emitted power to the total emitted power for the extended band. (c) The same format as for panel (a), for the short band. (d) The same format as for panel (b), for the short band.

for $F_{10.7}$) and decreasing post peak. The total UV power appears to be controlled by solar activity, with similar trends across the three indices showing comparable behavior to that of the Hisaki and Cassini (70–148 nm) powers. Broadfoot et al. (1981) also found that the intensity of the H_2 bands exhibited comparable behaviors to those observed in the solar fluxes at that time.

To quantitatively demonstrate the solar activity dependence, a Pearson correlation coefficient is determined for the Hisaki and Cassini powers (in both wavelength ranges) for total (north aurora and dayglow from the disk) and disk only with each of the solar activity indices, displayed in Table 1. There is no correlation coefficient for the Cassini UVIS extended band compared to solar EUV power, as the solar EUV power is determined for the short band wavelength range. The Hisaki correlation coefficients demonstrate a strong correlation between the solar activity and the total power. Comparatively, the total Cassini power in the same wavelengths indicates a weaker relationship than that of Hisaki; this may be a result of the auroral contribution detected by Cassini UVIS and the potential for remnant geocoronal contamination in the reduced Hisaki data, which will react strongly to solar activity (Waldrop & Paxton, 2013). To determine if the variability in the planetary dayglow emission is being driven by solar activity, the disk emission power is separated from the total power for the Cassini observations. The Cassini disk powers in the short band show a correlation coefficient of >0.8, confirming the solar activity control of the disk emission and that the auroral contribution makes a detectable impact on the total power (discussed later). Additionally, the Pearson correlation coefficients for the extended band Cassini power and disk only power are determined. They demonstrate an even stronger solar activity control, with correlation coefficients of >0.9.

The marginal differences in the temporal variability and dependence on the solar activity between the different wavelength ranges is an interesting point to examine. The differences between the two selected Cassini wavelength ranges is indicative of a stronger response of some H_2 bands to the solar UV spectrum than others. The extended wavelength range for Cassini employed in this study is determined by spectrally integrating over

Table 1
Pearson Correlation Coefficients for the Determined Powers and Solar Activity Proxies

Variable	Solar power	$F_{10.7}$ index	Solar H-Lyman β
Hisaki Power	0.757	0.788	0.752
Total Cassini Power (70–148 nm, short band)	0.551	0.523	0.528
Disk Cassini Power (70–148 nm, short band)	0.849	0.833	0.824
Total Cassini Power (70–170 nm, extended band)	–	0.966	0.956
Disk Cassini Power (70–170 nm, extended band)	–	0.964	0.949

155–162 nm and multiplying by 8.1. This spectral band contains the P(1) line of the H_2 Lyman band (6, 13) at 160.8 nm, which corresponds to fluorescence induced by solar H-Lyman β excitation. Liu and Dalgarno (1996), in their analysis of Jupiter's atmosphere and dayglow, modeled the solar-induced fluorescence spectrum of H_2 and demonstrated that solar H-Lyman β pumping produces the most intense fluorescence in the (6, 13) Lyman band, with a brightness of 48.7 R. The 155–162 nm band also includes the P(1) line of the (6, 12) Lyman band at 158.1 nm, another feature excited by solar H-Lyman β pumping, with a modeled brightness of 10.5 R. While Liu and Dalgarno (1996) focussed on jovian dayglow, they give a good indication of what processes could be responsible for the Saturn UV dayglow. Furthermore, the brightnesses of the (6, 13) Lyman band in Figure 9 of Gustin et al. (2010) indicates a greater contribution from solar fluorescence than photoelectron impact excitation. This effect is evident from the extended band Cassini power and H-Lyman β irradiance correlation coefficient, which is larger than that of the short band. While the solar H-Lyman β pumping also induces fluorescence within 70–148 nm, a larger proportion of the emission occurs longward of this range. The wavelength of the emitted photon from atmospheric hydrogen can be the same as the solar photon inducing the emission (resonant scattering), or larger (fluorescent scattering). In this case, solar H-Lyman β (102.5 nm) induces a stronger response via fluorescent scattering particularly at wavelengths >158 nm.

Gustin et al. (2010) investigated Saturn FUV dayglow, utilizing limb FUV Cassini UVIS spectra and comparing to synthetic H_2 spectra, to assess the contributions of photoelectron impact excitation and solar fluorescence in the dayglow emissions. They found the average contribution of photoelectron impact excitation was greater than the solar fluorescence over their FUV wavelength range, and that the photoelectrons likely had lower energy (tens of eV). They further suggest that solar fluorescence is more important on the disk than the limb, with electron impact excitation becoming increasingly more important at higher altitudes. The H_2 UV emitted powers determined from Hisaki observations and the H_2 Cassini emitted disk powers employed in this study convey that photo-ionization and subsequent electron impact excitation, and solar fluorescence are likely responsible for the majority of the emission and that the rate of these reactions are controlled by the rate of solar photons being delivered to the atmosphere. The Cassini disk powers are determined using pixels on the disk and away from the limb; the strong correlation with solar H-Lyman β pumping is supportive of solar fluorescence as one of the mechanisms for the H_2 dayglow.

3.4. Auroral Contribution and Variability

Another aim of this study is to assess the contribution of the aurora to the overall emitted power. With the Cassini imagery, it is possible to isolate the northern hemisphere auroral emission from the dayglow. The auroral power for the short band (Figure 5c), calculated as described in Section 2.2, is compared to the total power from the disk to determine the contribution. Figure 5d presents the contribution of the northern auroral power to the total power as a percentage. It is clear that the emitted power is dominated by that of the disk component, with the maximum contribution from the northern aurora reaching ~26% on 2014 DOY 149. The auroral power is also highest on this day, reaching 26.2 ± 4.6 GW. The contribution of the aurora is >10% across the interval and the variation of auroral power is detectable in the total emitted power trend.

The auroral activity appears variable, with greater activity on 2014 DOY 145, 149, and 162 indicated by the increased mean values and standard deviations. The solar wind dynamic pressure, propagated to Saturn using the Tao propagation model (Tao et al., 2005), shows a possible solar wind compression during DOY 143, but it is possible that it coincides with an auroral brightening on DOY 145 due to the uncertainty in modeled arrival time.

For Jupiter, the uncertainty was estimated at 19.7 hr for Jupiter-Sun-Earth angles of <50° (Tao et al., 2005). During this interval the Saturn-Sun-Earth angle was <50°; while also considering the increased propagation distance, it is sensible to estimate an uncertainty in arrival time of at least 24 hr. This indicates the possibility of solar wind compression-induced brightening on this day, as has been revealed by past studies (Badman et al., 2016; Nichols et al., 2014; Prangé et al., 2004). While the solar wind then remains quiet for the remainder of the interval, internal processes were likely occurring and influencing the auroral activity. Internal transport processes and plasma loading are constantly occurring and large-scale plasma injections have been frequently observed to influence the aurora (Bader, Badman, Cowley, et al., 2019; Kinrade et al., 2020; Mitchell et al., 2009).

Despite being unable to separate the disk and auroral components with Hisaki, it is likely that Hisaki is detecting mostly dayglow emission on the disk. However, there is a coincident increase in the emitted power on DOY 149 with no corresponding increase in solar activity that could indicate a detection of higher auroral activity as seen in the Cassini UVIS observations.

The same process of separating the auroral contribution is repeated for the extended band. The extended band auroral powers (Figure 5a) show similar temporal behavior to the short band auroral powers (Figure 5c), with several auroral brightenings observed. The peak power also occurs on 2014 DOY 149, at 85.4 ± 26.5 GW, a factor of 3.4 greater than that in the short band, and contributing 13.9%. Overall, the contribution by the aurora is ∼2%–14% over the interval, and the temporal behavior is dominated by that of the dayglow. This behavior is indicative of attenuation by hydrocarbon absorption reducing the auroral emitted power in the shorter wavelengths, due to the thermospheric hydrocarbon layer interacting with the auroral emitting layer (Gustin et al., 2012). Previously, Bader, Badman, Cowley et al. (2019) examined the 2014 DOY 145–162 sequence of projected auroral imagery in order to quantify the auroral UV power and constrain spatial and temporal behavior. The auroral powers determined in this study from unprojected imagery show comparable temporal behavior, with quiet activity observed on DOY 147, 158, and 159 as found by Bader, Badman, Cowley, et al. (2019). Furthermore, the UV auroral power per pseudoimage presented in Figure 4 of Bader, Badman, Cowley, et al. (2019) demonstrates a maximum of ∼90 GW during DOY 162, comparable to the daily average value of 74.9 ± 35.1 GW.

3.5. Dayglow Brightness

The methodology for determining the dayglow is repeated using calibrated, projected Cassini UVIS imagery for total H_2 (Bader, Badman, Cowley, et al., 2019; Bader, Badman, Yao, et al., 2019) in order to determine the disk-average brightness for comparison to previous dayglow studies. From the Cassini UVIS imagery and interpolated dayglow, the dayside disk-averaged brightness (outside of the defined auroral region of >22° colatitude) in the H_2 bands ranges from 0.80 to 1.49 kR over the interval of interest. Broadfoot et al. (1981) reported an H_2 dayside disk intensity of 0.7 kR from Voyager 1 planetary spectra. Intensities obtained from Voyager 1 equatorial disk spectra by Shemansky and Ajello (1983) were estimated at 0.916 kR. Evaluation of spectra from Voyager 1 and Voyager 2 data obtained disk brightnesses of 0.92 and 1.08 kR, respectively (Yelle et al., 1986). Gustin et al. (2010) found that the limb-averaged brightness due to photoelectron impact was 1.054 kR, with solar fluorescence contributing 0.460 kR for a total H_2 limb dayglow brightness of 1.514 kR. The disk-average dayglow brightnesses reported here are in agreement with previous studies, but it is important to remember that much of the disk was modeled based on the SZA-brightness dependence. Even so, evaluation of disk brightness from the UVIS imagery only (outside of the auroral region) reveals values in the range ∼0.80–1.42 kR, which remains in agreement with previous estimates.

4. Conclusions

Coincident observations of Saturn in mid-2014 by Hisaki and Cassini have been analyzed to determine the temporal behavior of the H_2 UV emissions from the planet's disk-wide dayglow and northern aurora over an approximately three week interval. The solar activity dependence of the power, the contribution of the north aurora to the total power, and the comparison between separate instruments is presented. This study reports the

first analysis of the observations of Saturn by Hisaki, a determination of the emitted power from the dayglow on the entire planetary dayside disk, and its temporal behavior.

The Hisaki data are reduced to total emitted powers for 70–148 nm (excluding atomic H, N, O lines subject to geocoronal contamination); significant temporal variation is observed over the interval, strongly correlated with solar activity. Variation by a factor of 2.26 is observed, with a maximum power of 69.6 ± 3.8 GW on 2014 DOY 162.

Cassini UVIS data from the EUV and FUV channels are analyzed in the same wavelengths (short band) and for 70–170 nm (an extended band), separately, and the auroral component is separated. The total power in the short band demonstrates similar trends to those indicated by Hisaki. In this case, variation by a factor of 1.29 is observed, with a maximum power of 104.6 ± 6.1 GW on 2014 DOY 145. Despite the peak occurring on a different day than that of Hisaki, the auroral contribution was significant at ∼20%. The northern aurora contributes 10%–26% across the interval and is detectable in the temporal trend of the total power. The disk power in the extended band demonstrates a stronger correlation with the solar activity, indicating a stronger response of the longer wavelengths to the solar spectrum. The total power maximizes on 2014 DOY 162 at 897 ± 32 GW. The aurora demonstrates comparable temporal behavior to the short band but contributes only ∼2%–14%, which may be due to the stronger spectral response of the dayglow contribution to the solar spectrum. The auroral contribution is more significant in the short band; although the total power is dominated by the dayglow from the planetary disk, the aurora is contributing a significant enough fraction of the emission to be detectable. The total power is therefore dominated by the dayglow emission from the disk across the observation period.

The temporal behavior of the dayglow over a period of weeks displayed significant changes, correlated with the solar activity. Variation in the Cassini disk power responded within the day to changes in the solar activity, particularly in the extended band. It is likely that photo-ionization and subsequent low energy photoelectron impact excitation, and solar fluorescence are responsible for the majority of the emission, as demonstrated by previous studies. Cassini total emitted powers in the same wavelength range are a factor of 1.7 larger than Hisaki values but display similar temporal trends. The correlation coefficient between the Hisaki and Cassini total powers is 0.60 (a moderately positive value), despite some differences in temporal coverage, demonstrating that both of the instruments are tracking the variability. These results highlight the ability of Hisaki to successfully observe the UV emissions from Saturn and detect the temporal variability. The multi-mission comparison is an opportunity to consider improvements to UV instrumentation for even more successful observations by later space telescopes. For example, one limitation of Hisaki was its low-Earth orbit; the Earth's geocorona contaminated the data, and this is particularly an issue for a UV target like Saturn, due to larger observing distances and weaker UV emissions than Jupiter or Venus. Scientists in their proposal for LAPYUTA aim to reduce this contamination by placing the telescope in medium-Earth orbit, improving observation of solar system planetary atmospheres.

Appendix A: Hisaki UV Powers 2015

The Hisaki data used in this study is reduced according to the procedure outlined in Section 2.1. Additionally, we can calculate the emitted power during the 2015 observing campaign and compare to the same solar indices (Figure A1). It should be noted that the viewing geometry of Saturn in 2015 was not optimal, with the Sun-Earth-Saturn angle approaching 90°; there were often very low on-target integration times, resulting in the omission of some observations. There are no Cassini UVIS auroral or HST observations available for analysis and comparison for this interval. The correlation coefficients for the power and each of the solar activity indices are ∼0.35, indicating a weak but positive correlation. This could be a result of poor data quality and unideal viewing for this campaign.

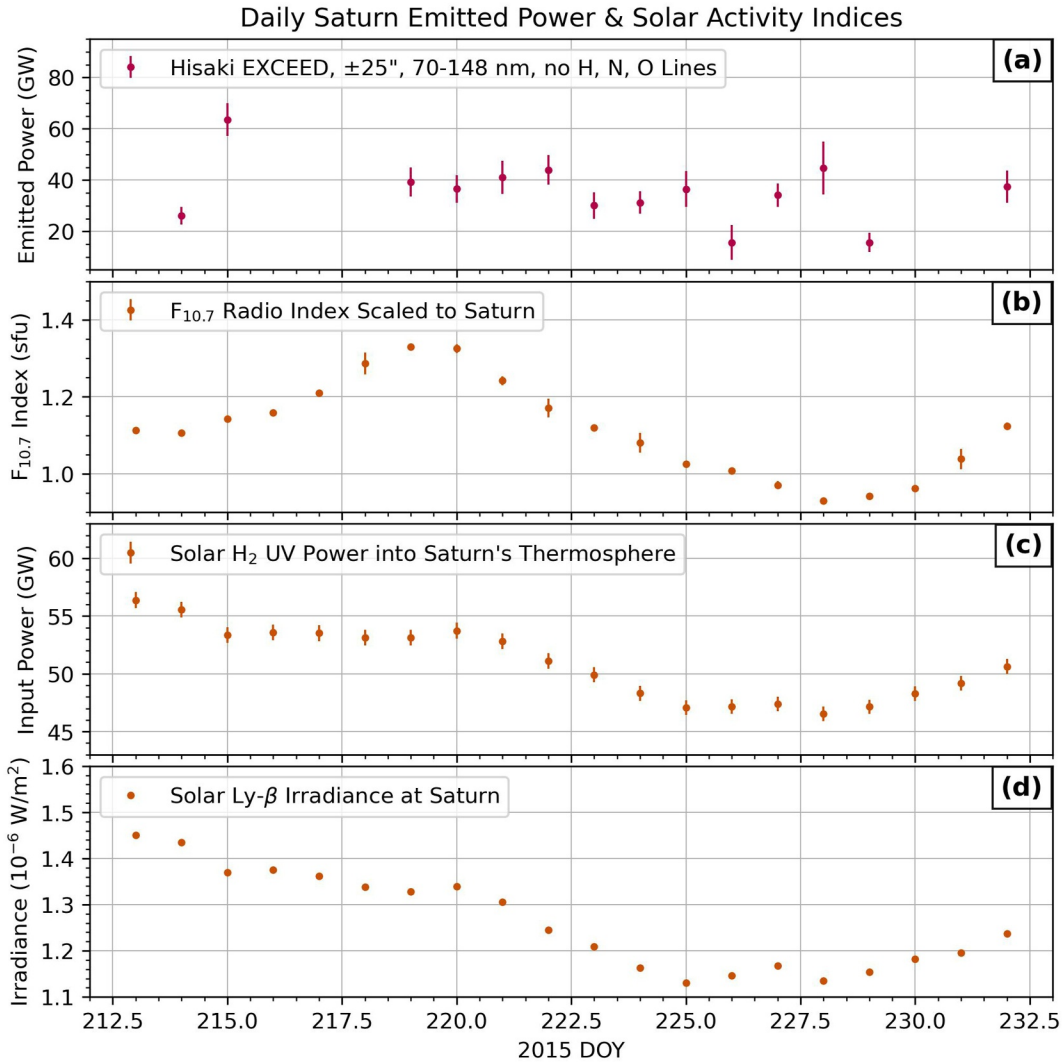

Figure A1. Summary of the total emitted H_2 power determined from the 2015 Hisaki campaign compared with the same solar proxies. (a) The total emitted UV power obtained from Hisaki/EXCEED. The points are daily average H_2 powers from 70 to 148 nm. ((b) The daily average solar $F_{10.7}$ radio index, scaled to Saturn. Data from Space Weather Canada. (c) The solar EUV power into Saturn's thermosphere. Solar spectral irradiance data are obtained from LISIRD. The calculation is from Gershman and DiBraccio (2024). (d) The solar H-Lyman β irradiance at Saturn; data are obtained from LISIRD, which uses the Flare Solar Irradiance Model (Chamberlin et al., 2008) and Earth irradiance measurements. The uncertainty on the solar H-Lyman β irradiance ranges from 24.7% to 28% over the interval.

Conflict of Interest

The authors declare no conflicts of interest relevant to this study.

Availability Statement

Cassini data are publicly available from the NASA Planetary Data System (https://pds.nasa.gov/). Information on Cassini UVIS data structure and guidance on calibration procedures can be found on the NASA PDS Atmospheres Node (https://pds-atmospheres.nmsu.edu/data_and_services/atmospheres_data/Cassini/inst-uvis.html). Data from the Hisaki satellite are archived at the Data Archives and Transmission System (DARTS) JAXA (https://data.darts.isas.jaxa.jp/pub/hisaki/). The Hisaki data used in this study were reduced in the pipeline system developed by Kimura et al. (2019), and are available in the archive as Level-2 data products. Data for the solar

spectral irradiances at Saturn are obtainable from LISIRD: Laboratory for Atmospheric and Space Physics (LASP) Interactive Solar Irradiance Datacenter (https://lasp.colorado.edu/lisird/).

Acknowledgments
L. S. C. was funded by an STFC studentship (50%; ST/Y509292/1) and Lancaster University FST Studentship (50%). Discussion of this work was supported by a JSPS Postdoctoral Research Fellowship (Summer Programme). S. V. B. and J. K. were supported by STFC Grant ST/Y002393/1. T. K., C. T., and F. T. were supported by JSPS KAKENHI Grant 20KK0074.

References

Bader, A., Badman, S. V., Cowley, S. W., Yao, Z. H., Ray, L. C., Kinrade, J., et al. (2019). The dynamics of Saturn's main aurorae. *Geophysical Research Letters*, *46*(17–18), 10283–10294. https://doi.org/10.1029/2019GL084620

Bader, A., Badman, S. V., Yao, Z. H., Kinrade, J., & Pryor, W. R. (2019). Observations of continuous quasiperiodic auroral pulsations on Saturn in high time-resolution UV auroral imagery. *Journal of Geophysical Research: Space Physics*, *124*(4), 2451–2465. https://doi.org/10.1029/2018JA026320

Badman, S. V., Provan, G., Bunce, E. J., Mitchell, D. G., Melin, H., Cowley, S. W., et al. (2016). Saturn's auroral morphology and field-aligned currents during a solar wind compression. *Icarus*, *263*, 83–93. https://doi.org/10.1016/j.icarus.2014.11.014

Broadfoot, A. L., Herbert, F., Holberg, J. B., Hunten, D. M., Kumar, S., Sandel, B. R., et al. (1986). Ultraviolet spectrometer observations of Uranus. *Science*, *233*(4759), 74–79. https://doi.org/10.1126/science.233.4759.74

Broadfoot, A. L., Sandel, B. R., Shemansky, D. E., Holberg, J. B., Smith, G. R., Strobel, D. F., et al. (1981). Extreme ultraviolet observations from voyager 1 encounter with Saturn. *American Association for the Advancement of Science*, *212*(4491), 206–211. https://doi.org/10.1126/science.212.4491.206

Chamberlin, P. C., Woods, T. N., & Eparvier, F. G. (2008). Flare irradiance spectral model (FISM): Flare component algorithms and results. *Space Weather*, *6*(5). https://doi.org/10.1029/2007SW000372

Clarke, J. T., Gérard, J. C., Grodent, D., Wannawichian, S., Gustin, J., Connerney, J., et al. (2005). Morphological differences between Saturn's ultraviolet aurorae and those of Earth and Jupiter. *Nature*, *433*(7027), 717–719. https://doi.org/10.1038/nature03331

Clarke, J. T., Hudson, M. K., & Yung, Y. L. (1987). The excitation of the far ultraviolet electroglow emissions on Uranus, Saturn, and Jupiter. *Journal of Geophysical Research*, *92*(A13), 15139–15147. https://doi.org/10.1029/JA092iA13p15139

Clarke, J. T., Nichols, J., Gérard, J. C., Grodent, D., Hansen, K. C., Kurth, W., et al. (2009). Response of Jupiter's and Saturn's auroral activity to the solar wind. *Blackwell Publishing Ltd*, *114*(5). https://doi.org/10.1029/2008JA013694

Esposito, L. W., Barth, C. A., Colwell, J. E., Lawrence, G. M., Mcclintock, W. E., Ian, A., et al. (2004). The Cassini ultraviolet imaging spectrograph investigation. *Space Science Reviews*, *115*(1–4), 299–361. https://doi.org/10.1007/s11214-004-1455-8

Gérard, J. C., Grodent, D., Gustin, J., Saglam, A., Clarke, J. T., & Trauger, J. T. (2004). Characteristics of Saturn's FUV aurora observed with the space telescope imaging spectrograph. *Journal of Geophysical Research: Space Physics*, *109*(A9). https://doi.org/10.1029/2004JA010513

Gershman, D. J., & DiBraccio, G. A. (2024). Quantifying external energy inputs for giant planet magnetospheres. *Geophysical Research Letters*, *51*(15), e2024GL109660. https://doi.org/10.1029/2024GL109660

Groulard, A., Bonfond, B., Grodent, D., Gérard, J. C., Greathouse, T. K., Hue, V., et al. (2024). Dawn-dusk asymmetry in the main auroral emissions at Jupiter observed with Juno-UVS. *Icarus*, *413*, 116005. https://doi.org/10.1016/j.icarus.2024.116005

Gustin, J., Bonfond, B., Grodent, D., & Gérard, J. C. (2012). Conversion from HST ACS and STIS auroral counts into brightness, precipitated power, and radiated power for H_2 giant planets. *Journal of Geophysical Research: Space Physics*, *117*(7). https://doi.org/10.1029/2012JA017607

Gustin, J., Feldman, P. D., Gérard, J. C., Grodent, D., Vidal-Madjar, A., Jaffel, L. B., et al. (2004). Jovian auroral spectroscopy with FUSE: Analysis of self-absorption and implications for electron precipitation. *Icarus*, *171*(2), 336–355. https://doi.org/10.1016/j.icarus.2004.06.005

Gustin, J., Grodent, D., Radioti, A., Pryor, W., Lamy, L., & Ajello, J. (2017). Statistical study of Saturn's auroral electron properties with Cassini/UVIS FUV spectral images. *Icarus*, *284*, 264–283. https://doi.org/10.1016/j.icarus.2016.11.017

Gustin, J., Grodent, D., Ray, L. C., Bonfond, B., Bunce, E. J., Nichols, J. D., & Ozak, N. (2016). Characteristics of north Jovian aurora from STIS FUV spectral images. *Icarus*, *268*, 215–241. https://doi.org/10.1016/j.icarus.2015.12.048

Gustin, J., Stewart, I., Gérard, J. C., & Esposito, L. (2010). Characteristics of Saturn's FUV airglow from limb-viewing spectra obtained with Cassini-UVIS. *Icarus*, *210*(1), 270–283. https://doi.org/10.1016/j.icarus.2010.06.031

Kimura, T., Badman, S. V., Tao, C., Yoshioka, K., Murakami, G., Yamazaki, A., et al. (2015). Transient internally driven aurora at Jupiter discovered by Hisaki and the Hubble space telescope. *Geophysical Research Letters*, *42*(6), 1662–1668. https://doi.org/10.1002/2015GL063272

Kimura, T., Yamazaki, A., Yoshioka, K., Murakami, G., Tsuchiya, F., Kita, H., et al. (2019). Development of ground pipeline system for high-level scientific data products of the Hisaki satellite mission and its application to planetary space weather. *Journal of Space Weather and Space Climate*, *9*, A8. https://doi.org/10.1051/swsc/2019005

Kinrade, J., Badman, S. V., Paranicas, C., Mitchell, D. G., Arridge, C. S., Gray, R. L., et al. (2020). Tracking counterpart signatures in Saturn's auroras and ENA imagery during large-scale plasma injection events. *Journal of Geophysical Research: Space Physics*, *125*(2), e2019JA027542. https://doi.org/10.1029/2019ja027542

Kita, H., Kimura, T., Tao, C., Tsuchiya, F., Murakami, G., Yamazaki, A., et al. (2019). Jovian UV Aurora's response to the solar wind: Hisaki EXCEED and Juno observations. *Journal of Geophysical Research: Space Physics*, *124*(12), 10209–10218. https://doi.org/10.1029/2019JA026997

Koskinen, T. T., Sandel, B. R., Yelle, R. V., Holsclaw, G. M., & Quemerais, E. (2020). Saturn in Lyman α: A comparison of Cassini and Voyager observations. *Icarus*, *339*, 113594. https://doi.org/10.1016/j.icarus.2019.113594

Lamy, L., Prangé, R., Pryor, W., Gustin, J., Badman, S. V., Melin, H., et al. (2013). Multispectral simultaneous diagnosis of Saturn's aurorae throughout a planetary rotation. *Journal of Geophysical Research: Space Physics*, *118*(8), 4817–4843. https://doi.org/10.1002/jgra.50404

Liu, W., & Dalgarno, A. (1996). The ultraviolet spectrum of the Jovian dayglow. *The Astrophysical Journal*, *462*, 502–518. https://doi.org/10.1086/177168

McGrath, M. A., & Clarke, J. T. (1992). H I Lyman alpha emission from Saturn (1980–1990). *Journal of Geophysical Research*, *97*(A9), 13691–13703. https://doi.org/10.1029/92ja00143

Melin, H., Shemansky, D. E., & Liu, X. (2009). The distribution of atomic hydrogen and oxygen in the magnetosphere of Saturn. *Planetary and Space Science*, *57*(14–15), 1743–1753. https://doi.org/10.1016/j.pss.2009.04.014

Mitchell, D. G., Krimigis, S. M., Paranicas, C., Brandt, P. C., Carbary, J. F., Roelof, E. C., et al. (2009). Recurrent energization of plasma in the midnight-to-dawn quadrant of Saturn's magnetosphere, and its relationship to auroral UV and radio emissions. *Planetary and Space Science*, *57*(14–15), 1732–1742. https://doi.org/10.1016/j.pss.2009.04.002

Nichols, J. D., Badman, S. V., Baines, K. H., Brown, R. H., Bunce, E. J., Clarke, J. T., et al. (2014). Dynamic auroral storms on Saturn as observed by the Hubble space telescope. *Geophysical Research Letters*, *41*(10), 3323–3330. https://doi.org/10.1002/2014GL060186

Nichols, J. D., Badman, S. V., Bunce, E. J., Clarke, J. T., Cowley, S. W., Crary, F. J., et al. (2009). Saturn's equinoctial auroras. *Geophysical Research Letters*, *36*(24). https://doi.org/10.1029/2009GL041491

Prangé, R., Pallier, L., Hansen, K. C., Howard, R., Vourlidas, A., Courtin, R., & Parkinson, C. (2004). An interplanetary shock traced by planetary auroral storms from the Sun to Saturn. *Nature*, *432*(7013), 78–81. https://doi.org/10.1038/nature02986

Shemansky, D. E., & Ajello, J. M. (1983). The Saturn spectrum in the EUV-electron excited hydrogen. *Journal of Geophysical Research*, *88*(A1), 459–464. https://doi.org/10.1029/ja088ia01p00459

Stephenson, P., Koskinen, T. T., Brown, Z., Quémerais, E., Lavvas, P., Moses, J. I., et al. (2024). Seasonal variation of Saturn's Ly α brightness. *The Astrophysical Journal*, *971*(1), 89. https://doi.org/10.3847/1538-4357/ad50a6

Tao, C., Kataoka, R., Fukunishi, H., Takahashi, Y., & Yokoyama, T. (2005). Magnetic field variations in the Jovian magnetotail induced by solar wind dynamic pressure enhancements. *Journal of Geophysical Research: Space Physics*, *110*(A11). https://doi.org/10.1029/2004JA010959

Tobiska, W. K., Bouwer, S. D., & Bowman, B. R. (2008). The development of new solar indices for use in thermospheric density modeling. *Journal of Atmospheric and Solar-Terrestrial Physics*, *70*(5), 803–819. https://doi.org/10.1016/j.jastp.2007.11.001

Tsuchiya, F., Murakami, G., Yamazaki, A., & Kameda, S. (2026). Future ultraviolet space telescope mission LAPYUTA. https://doi.org/10.5194/egusphere-egu26-21086

Tsuchiya, F., Murakami, G., Yamazaki, A., Kameda, S., Kimura, T., Koga, R., et al. (2024). Overview of the LAPYUTA mission (Life-environmentology, astronomy, and PlanetarY Ultraviolet telescope assembly). In J.-W. A. den Herder, K. Nakazawa, & S. Nikzad (Eds.), *Space telescopes and instrumentation 2024: Ultraviolet to gamma ray*. SPIE. https://doi.org/10.1117/12.3017298

Waldrop, L., & Paxton, L. J. (2013). Lyman α airglow emission: Implications for atomic hydrogen geocorona variability with solar cycle. *Journal of Geophysical Research: Space Physics*, *118*(9), 5874–5890. https://doi.org/10.1002/jgra.50496

Yamazaki, A., Tsuchiya, F., Sakanoi, T., Uemizu, K., Yoshioka, K., Murakami, G., et al. (2014). Field-of-view guiding camera on the HISAKI (SPRINT-A) satellite. *Kluwer Academic Publishers*, *184*(1–4), 259–274. https://doi.org/10.1007/s11214-014-0106-y

Yelle, R. V. (1988). H_2 emissions from the outer planets. *Geophysical Research Letters*, *15*(10), 1145–1148. https://doi.org/10.1029/GL015i010p01145

Yelle, R. V., McConnell, J. C., Sandel, B. R., & Broadfoot, A. L. (1987). The dependence of electroglow on the solar flux. *Journal of Geophysical Research*, *92*(A13), 15110–15124. https://doi.org/10.1029/ja092ia13p15110

Yelle, R. V., Sandel, B. R., Shemansky, D. E., & Kumar, S. (1986). Altitude variation of EUV emissions and evidence for proton precipitation at low latitudes in the Saturnian atmosphere. *Journal of Geophysical Research*, *91*(A8), 8756–8770. https://doi.org/10.1029/ja091ia08p08756

Yoshikawa, I., Yoshioka, K., Murakami, G., Yamazaki, A., Tsuchiya, F., Kagitani, M., et al. (2014). Extreme ultraviolet radiation measurement for planetary atmospheres/magnetospheres from the earth-orbiting spacecraft (extreme ultraviolet spectroscope for exospheric dynamics: EXCEED), In *Space Science Reviews* (Vol. 184(1–4), pp. 237–258). Kluwer Academic Publishers. https://doi.org/10.1007/s11214-014-0077-z

Yoshioka, K., Murakami, G., Yamazaki, A., Tsuchiya, F., Kagitani, M., Sakanoi, T., et al. (2013). The extreme ultraviolet spectroscope for planetary science. *EXCEED. Planetary and Space Science*, *85*, 250–260. https://doi.org/10.1016/j.pss.2013.06.021